Materials Transactions, Vol. 46, No. 10 (2005) pp. 2204 to 2210

Gas Pore Formation in Lost Foam Casting of AZ91H Mg Alloy in Comparison with A356 Al Alloy

Seung-Ryoul Shin[1], Sang-Won Han[1,*] and Kyong-Whoan Lee[2]

[1]*Department of Materials Science and Engineering, KAIST, 373-1 Guseong-dong, Yuseong-gu, Daejeon, 305-701, Korea*
[2]*Korea Institute of Industrial Technology, 472 Kajwa 4-dong, Seo-ku, Incheon 404-254 Korea*

Castings performed under reduced pressure and atmosphere were used to investigate the formation of pores in lost foam casting (LFC) of the AZ91H Mg alloy, and the results are compared with the results of a previous work on the A 356 Al alloy.

In LFC, although the pouring temperature of the AZ91H alloy melt was higher than that of the A356 alloy, the amount of porosity in the AZ91H alloy after solidification was much lower than that of the A356 alloy. The lower porosity was caused by the extra hydrogen solubility. The pore formation mechanism of the AZ91H alloy in LFC was similar to that of the A356 alloy but the critical temperature for generating a different mechanism of pore formation is higher in the A356 alloy by as much as about 323 K. The mold evacuation promotes lower porosity and shrinkage defects due to the easy removal of polystyrene products. However, the exceeded vacuum degree severely entraps polymer pyrolysis products, thereby leaving large pores after solidification.

(Received June 13, 2005; Accepted August 10, 2005; Published October 15, 2005)

Keywords: *lost foam casting, pore formation, AZ91H alloy, A356 alloy, entrapment of pyrolysis products*

1. Introduction

The application of lost foam casting (LFC), which was invented by Shroyer in 1950, is increasing worldwide because it can form casts with a complex shape without sand binders.[1)] LFC has been mainly used to make automobile parts such as intake manifolds, brake pump housings, cylinder heads, and engine blocks of aluminum and ferrous alloys. However, LFC has not been successfully applied to the Mg alloy, though the Mg alloy has many distinct advantages over other construction materials, such as low density, high modulus, good machinability and availability, and is also used in the production of light-weight industrial components.

The problem of applying LFC to the Mg alloy is likely due to the Mg alloy's poor fluidity and the possibility of a chemical reaction between the Mg alloy melt and the pattern material. Fluidity is generally measured as the flow length of the melt at a certain pouring temperature and pressure. The poor fluidity of the Mg alloy is due to its low density, low heat capacity and latent heat. In addition, in LFC, the fluidity of the Mg alloy may decrease remarkably because of the heat loss of the front of the melt, which is caused by the endothermic reaction during the decomposition of the pattern.

In addition, carbon dioxide of gas type deteriorates the chemical reactivity between the Mg alloy melt and the pattern material.[2)] Thus, to improve the fluidity of the Mg alloy melt during LFC, the air must be evacuated from the mold.

The polystyrene that we used as the pattern of the LFC consisted of 92 mass% C and 8 mass% H.[3–5)] The C_6H_5 benzene ring in the polystyrene was stable and the –CH=CH2– chain tended to decompose first. The benzene ring remained in the liquid phase and reacted with the melt to cause casting defects. At 973 K, 60 percent of the polystyrene decomposed into the liquid phase melt, causing an increase in casting defects.

The reaction between the alloy melt and the liquid polymers produces many reaction products, which, in turn, cause casting defects. We previously confirmed, for example, that the gas phase generated by the polymer in LFC of A356 is a factor in the formation of pores.[6,7)] However, few studies have focused on the LFC of the Mg alloy, especially in relation to casting defects. Thus, we investigated the formation of pores in the LFC of the AZ91H alloy and compared the results with a previous work on the A 356 alloy.

2. Experimental Details

2.1 Reduced pressure test and hydrogen content calculation

To investigate the hydrogen gas content in an AZ91H alloy ingot after the reaction of the AZ91H alloy melt and polystyrene, we used reduced pressure casting. Figure 1 shows a schema of the test apparatus. First, we prepared a stainless steel cup with a thickness of 1 mm and a volume of 170 cm^3. We then coated the cup with a 0.2 mm layer of BN powder and preheated it to 473 K. After placing the cup in the chamber, we inserted a different amount of expanded polystyrene (EPS) into the cup. We then poured about 100 g of the AZ91H alloy melt into the cup. The glass cover was then closed and the chamber was immediately evacuated to the optimal reduced pressure, 21 kPa, which gave a reproductive and consistent hydrogen gas content for the same amount of melt.[6–8)]

The final set pressure was taken after 5 s, and the melt solidified after about 8 min. The gasification of the EPS took several seconds after we poured the melt into the cup with the EPS. The used melts were a non-degassed melt and a degassed melt. For the degassing, we used Ar gas with a flow rate of 5.0 L/min for 30 min.

To calculate the bulk density (ρ_b) and the total porosity,

*Corresponding author, E-mail: hsw33@kaist.ac.kr

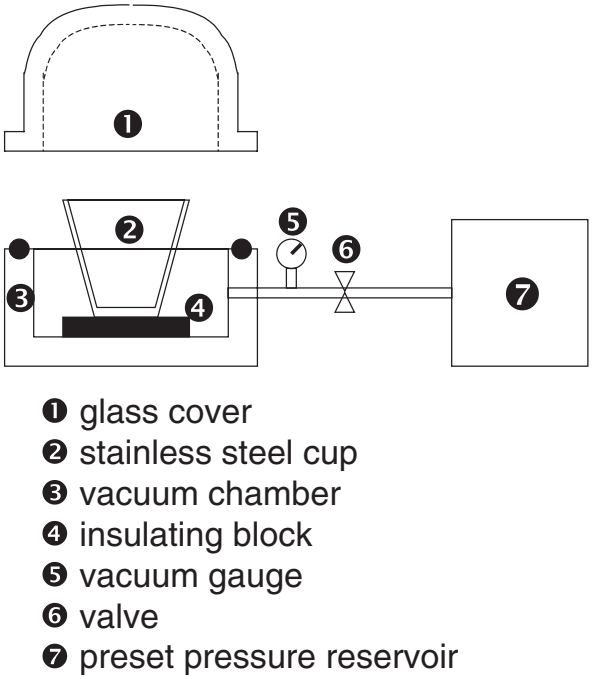

Fig. 1 Schematic apparatus of reduced pressure test set.

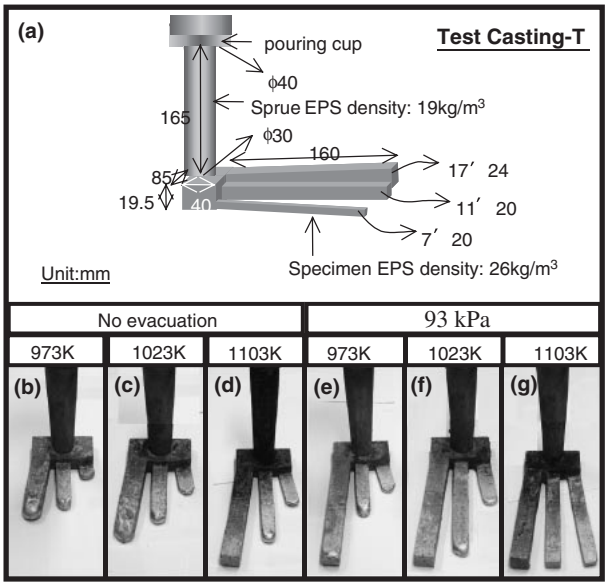

Fig. 2 (a) The shape of the Test Casting-T manufactured by lost foam casting (unit:mm); (a) dimension of casting; (b)–(g) shape of each casting for AZ91H alloy under various casting conditions.

which includes open pores on the severed surface of the sample, we used the following equations:

$$\rho_b = (W_d \times \rho_w)/(W_s - W_b) \quad (g/cm^3) \tag{1}$$

$$\text{Porosity in vol\%} = [1 - (\rho_b/\rho_{th})] \times 100 \tag{2}$$

where

W_d = dry mass
W_b = suspended mass in water
W_s = mass with open pores filled with water (wetted mass)
ρ_{th} = theoretical density of the A356 alloy = 2.658 g/cm^3
ρ_w = density of water.

We then used the density results of eq. (1) to calculate the hydrogen content in the melt, C_H, from eq. (3). Moreover, we assumed that all the observed pores constituted the total hydrogen content that formed at the solidus temperature under ambient pressure.[6–8] Equation (3) is expressed as

$$C_H[\text{mL } H_2/100\,\text{g Al}] = [(P_2/P_1) \times (T_1/T_2)] \times 100 \times [(1/\rho_b) - (1/\rho_{th})] \tag{3}$$

where

P_2 = the pressure during solidification (here 34 kPa)
P_1 = 100 kPa
T_2 = the alloy solidus temperature in K
T_1 = 273 K.

2.2 Lost foam casting

The casting design shown in Fig. 2 (Test Casting-T) was made to examine the hydrogen gas pickup during the LFC. The foam pattern for the Test Casting-T, which has three legs of different thickness (17, 11, and 7 mm), was coated with a 0.18 mm layer of a commercial coating material (EBA-COTE). We glued the legs to the sprue base, and then dried the coated pattern and place it in a flask.

After surrounding the pattern with sand, we employed mechanical vibration to densely compact the sand. The upper part of the flask was sealed to inhibit the leakage of vacuum. We then poured the AZ91H alloy melt into the pouring cup of the foam sprue at various pouring temperatures. For the evacuation, we maintained a pressure of 93 kPa in the flask during solidification.

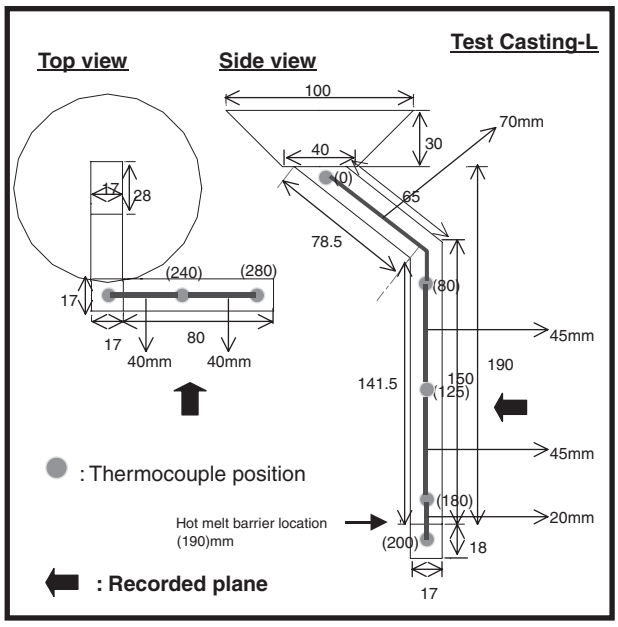

Fig. 3 Shape of test casting-L to visualize the filling behavior of the melt during LFC.

To investigate the formation of the pores, we used EDS analysis for the gas pore surfaces of the cast sample. Figure 3 shows the pattern (Test Casting-L) of the flow behavior of the AZ91H alloy melt during the LFC. Except for the pattern plane that was in contact with the quartz window, we coated all planes with a layer of up to 0.2 mm of a refractory material.

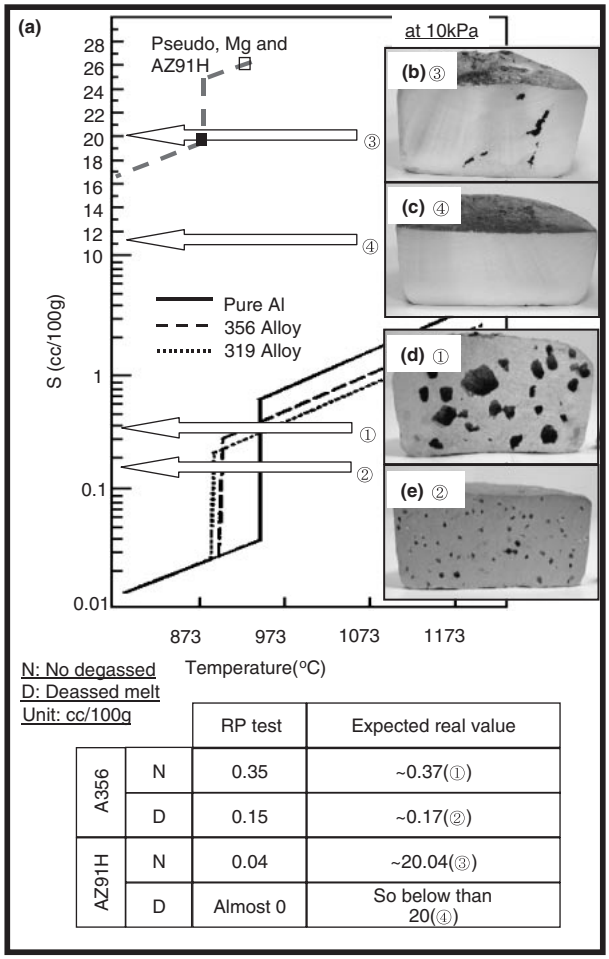

		RP test	Expected real value
A356	N	0.35	~0.37(①)
	D	0.15	~0.17(②)
AZ91H	N	0.04	~20.04(③)
	D	Almost 0	So below than 20(④)

Fig. 4 (a) The pseudo hydrogen solubility diagram of AZ91H alloy compared with that of A356 alloy; below table shows the measured hydrogen concentration for AZ91H alloy and A356 alloy by reduced pressure test and the expected real hydrogen concentration in the melts for both alloys, (b–e) photographs showing the polished surfaces of reduced pressure test samples; (b–c) AZ91H alloy and (d–e) A356 alloy.

The melt flow was monitored with a high-resolution digital camera. We then investigated the evacuation effects on the fluidity and porosity under various evacuation pressures (100, 93, 90, 80, 70, 60 and 50 kPa) in the Test Casting-T. The pouring was consistently performed at 983 K.

3. Results and Discussion

3.1 Reduced pressure casting without lost foam

Figures 4(b)–(c) and (d)–(e) show the cut surfaces of the AZ91H and A356 alloy samples of the reduced pressure cast (RP test) under a pressure of 100 k. The dissolved hydrogen content of the A356 alloy was 0.35 mL per 100 g of melt for the non-degassed melt, and about 0.15 mL per 100 g melt for the degassed melt.[7] The AZ91H alloy had much lower dissolved hydrogen content than the A356 alloy. The hydrogen content in the AZ91H alloy ingot was about 0.04 mL per 100 g of melt for the non-degassed melt, and about 0 mL per 100 g of melt for the degassed melt. Theoretically, other references on pure Mg and Mg alloys indicate that the AZ91H alloy must have a higher level of hydrogen solubility than the A 356 alloy.[9] However, the high hydrogen solubility limits in pure Mg and Mg alloys were obtained when the saturation hydrogen level in the chamber was purged by hydrogen.[10,11] For the hydrogen solubility of the AZ91H alloy under reduced pressure, we presumed on the basis of the hydrogen solubility mentioned in the references that there was pseudo solubility in Fig. 4(a). Similarly, we calculated the expected hydrogen solubility (for the expected real value) as shown in the table of Fig. 4.

To obtain the hydrogen content of the AZ91H alloy, we used a chamber of 80 percent humidity to mimic the chamber purged by hydrogen. As a result, the practical hydrogen content in the commercial AZ91H alloy ingot may have been much lower. On the other hand, by changing the mass of the polystyrene in the mold, the porosity volume increased sensitively in the A356 alloy but increased slightly for the AZ91H alloy. This reaction of the AZ91H alloy is likely due to the extra solubility of the melt for hydrogen, as explained in Fig. 4. That is, because of the high hydrogen solubility of the AZ91H melt, the hydrogen pores become solute into the melt even if many pores are formed.

3.2 Hydrogen gas pickup during the LFC

Figure 5(a) shows the change of porosity in the legs of the Casting-T sample with the largest cross section (17 mm × 24 mm); the melt was poured with various temperatures. Horizontal axis of Fig. 5(a) means each range in length direction of the channel. The percentage of porosity in all the samples increased slightly with the progressing direction of the channel tip, which may be due to the increased contact time between the melt and the pattern. In addition, the mold evacuation lowers the level of porosity, and we obtained a

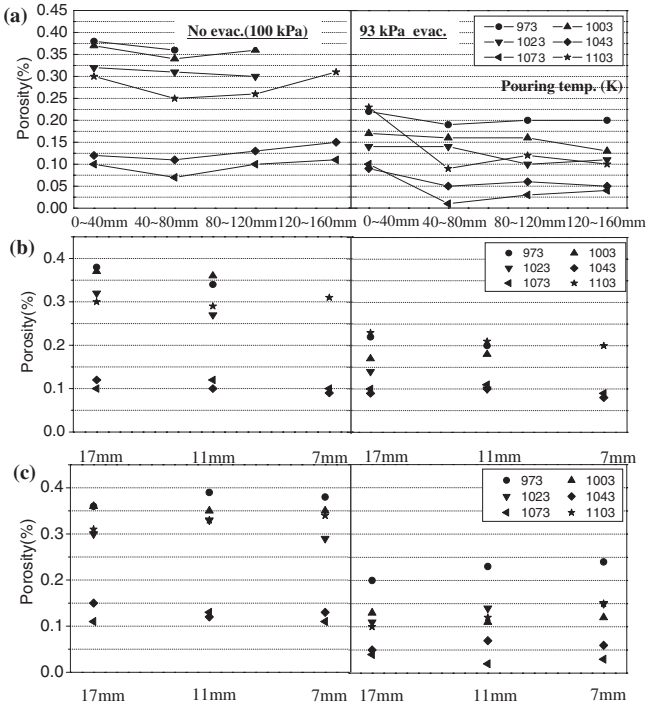

Fig. 5 (a) Porosity percent depending on pouring temperatures in the 17 mm-thick leg of Test Casting-T under evacuation (93 kPa) and no evacuation conditions for AZ91H alloy, (b) porosity variations in initial part (0–40 mm) of each channel, (c) porosity variations in the end part (120–160 mm) of each channel.

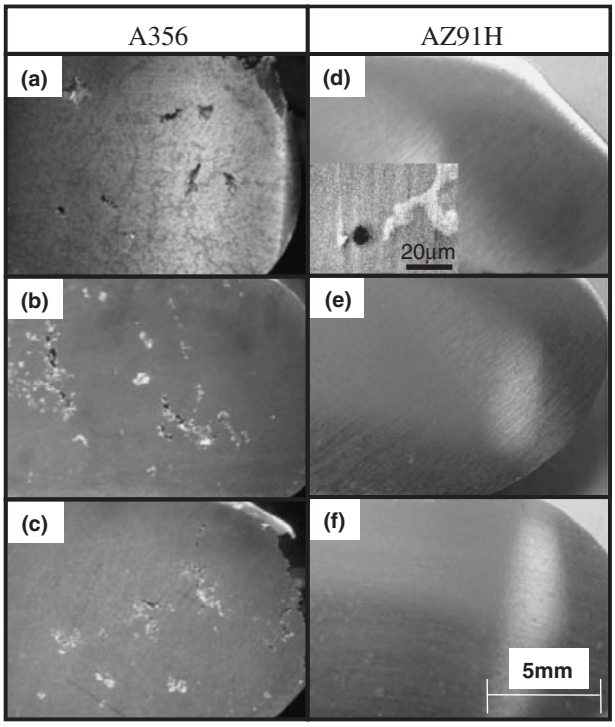

Fig. 6 Macrostructures in channel tip of 11 mm-thick legs; (a–c) A356 and (d–f) AZ91H alloys.

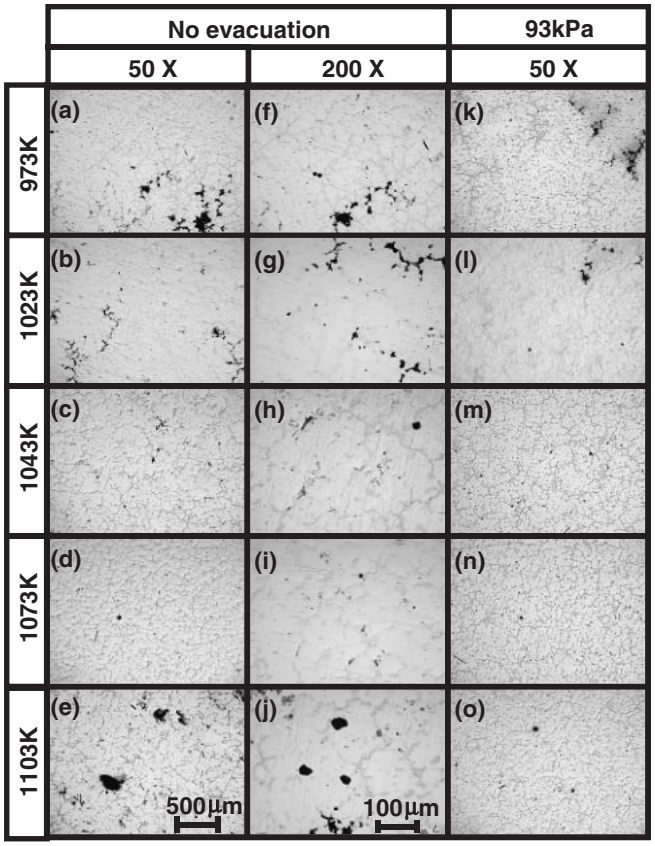

Fig. 7 Macrostructures in the channel tip of 17 mm-thick legs of AZ91H alloy with different pouring temperature and with-without evacuation.

minimum porosity of about 0.03 vol% at a pouring temperature of 1073 K. Figures 5(b)–(c) show the change of porosity at the initial part (0 to 40 mm) and the end part (120 to 160 mm) for the three kinds of channels thickness (17, 11, and 7 mm). The porosity in the initial part of the channel increased severely as the channel thickness increased from 0.4 to 1.05 vol% at 7 mm, from 0.6 to 1.2 vol% at 11 mm, and from 0.7 to 1.9 vol% at 17 mm. This increase resulted from the sprue effect in which the solidification time increases as the cast thickness increases. In contrast, the porosity at the end of the channel decreased as the channel thickness increased from 1.7 to 3.7 vol% at 7 mm, from 1.2 to 3.1 vol% at 11 mm, and from 0.8 to 2.2 vol% at 17 mm. This phenomenon may be due to the rapid cooling rate, which increases the entrapment of polystyrene pyrolysis products (especially liquid products).

Concerning change of porosity amount, similar behavior to the present study has been observed in the A356 alloy,[6,7] where the amount of porosity varied in a range of 0.6 to 2.2 vol%. However, in the case of the present AZ91H alloy, the change of porosity amount between the initial and end parts did not change very much from 0.05 to 0.4 vol%. in comparison with A356 alloy, showed a weak dependence on the channel thickness, as shown in Figs. 5(b)–(c). This weak dependence is likely due to the high extra solubility to hydrogen, as shown in Fig. 4, many porosity will be dissolved into AZ91H melt regardless of channel thickness of AZ91H alloy. Real decomposition process of porosity generating due to polystyrene pyrolysis products was shown in Figs. 9(c)–(h). The polystyrene channel is filled with AZ91H melt within 1.5 s after pouring [Fig. 9(d)]. In this time the melt contains a lot of porosity generating due to polystyrene pyrolysis products, the porosities was continuously contracted with holding time, almost disappeared after 25 s [Fig. 9(d)].

Figure 6 shows the macrostructure of the end of the channels for the A356 and AZ91H alloys. The pore size is about 1 mm and 10 μm in the middle-sized samples (11 mm × 20 mm) for both alloys, respectively. The large pores in the A356 alloy were primarily due to the entrapment of liquid products. Figure 7 shows the pore distribution in the AZ91H alloy with a 17 mm thick channel poured at different temperatures, with and without evacuation. For the A356 alloy, the minimum porosity of below 0.5 vol% was obtained at a pouring temperature of 1023 K.[6,7] In contrast, the porosity of the AZ91H alloy poured at 1073 K was only 0.5 vol%. This difference seems to be due to the fluidity of the AZ91H alloy, which was worse than that of the A356 alloy. The pore formation at low pouring temperatures is affected by shrinkage defects and the entrapment of liquid products [See Figs. 7(a)–(b)]; moreover, the pores at high pouring temperature seem to have originated from the entrapment of gaseous products and small liquid products in addition to the long solidification time [See Fig. 7(e)]. However, mold evacuation significantly lowers the pores and shrinkage defects as shown in Figs. 7(k)–(l). In LFC, pores can originate from different three mechanisms: entrapped liquid polymer, entrapped gaseous polymer and supersaturated hydrogen. In addition, the hydrogen gas can originate from the initial melt or from the reaction with the decomposed EPS. Differences in the carbon content vary according to the pore formation mechanisms. The carbon content of pores

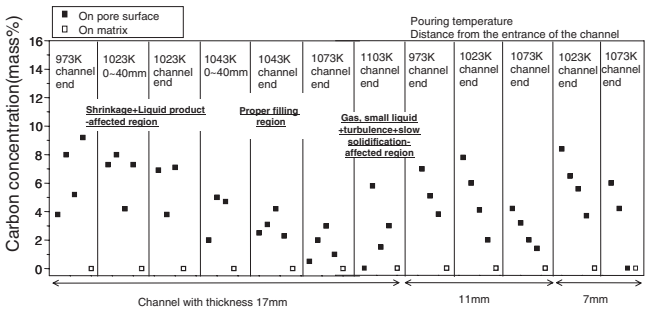

Fig. 8 Carbon concentrations in pores at different locations of test casting-T for AZ91H Mg alloy. The pouring temperature and specimen thickness and location are shown.

induced from entrapped liquid polymer are expected to be highest, and moderate or low levels of carbon are expected in pores induced from the entrapped gaseous polymer and the supersaturated hydrogen.

We analyzed the carbon content of the pore surface to know the origin of the pore; and Figure 8 shows the results of the analysis in 17 mm thickness channel. Several points indicating different carbon concentration were plotted in the same specimen. This means a mechanism does not act on pore generation, two or three mechanisms co-exist in the same specimen. The maximum carbon concentration and its overall level are important to judge main mechanism for pore generation. The maximum carbon concentration is about 9 mass% in samples poured at 973 K. This high carbon concentration means the pore originates from the entrapment of the liquid polymer products. The lowest carbon concentration can be generated from entrapped gaseous polymer and supersaturated hydrogen. Furthermore, the maximum carbon concentration consistently decreases down to about 4 mass% at a temperature of about 1073 K. This decrease means that the pore formation is governed by the entrapment of gaseous and small liquid products.

In the case of the A356 alloy, the maximum carbon concentration changed from 8 mass% at 973 K to 3 mass% at 1023 K.[6,7] That is, the transition between the pore formation mechanisms mentioned above takes place at 1023 K. The high transition temperature in the AZ91H alloy melt is likely due to the worse fluidity of the AZ91H alloy. Moreover, because of the difficulty of observing the pores with no carbon in the AZ91H alloy, the two entrapment mechanisms were dominant for pore formation. Conversely, many pores showed almost no carbon for the A356 alloy, though the carbon concentration in the matrix and size of the entrapped pyrolysis products for the AZ91H and A356 alloys is comparable.

The following three arguments explain the large difference in the porosity concentration of both alloys with the similar levels of carbon concentration. First, the thickness of the oxide film at the front of the liquid metal may inhibit the entrapment of the pyrolysis products. We measured the thickness at the tip of a broken sample with SEM. As shown in Figs. 9(a)–(b), the thickness of the oxide film was 586 nm for the AZ91H alloy and 331 nm for the A356 alloy. However, during the filling, the oxide film is easily broken by the turbulence of the melt and a new oxide film is formed;

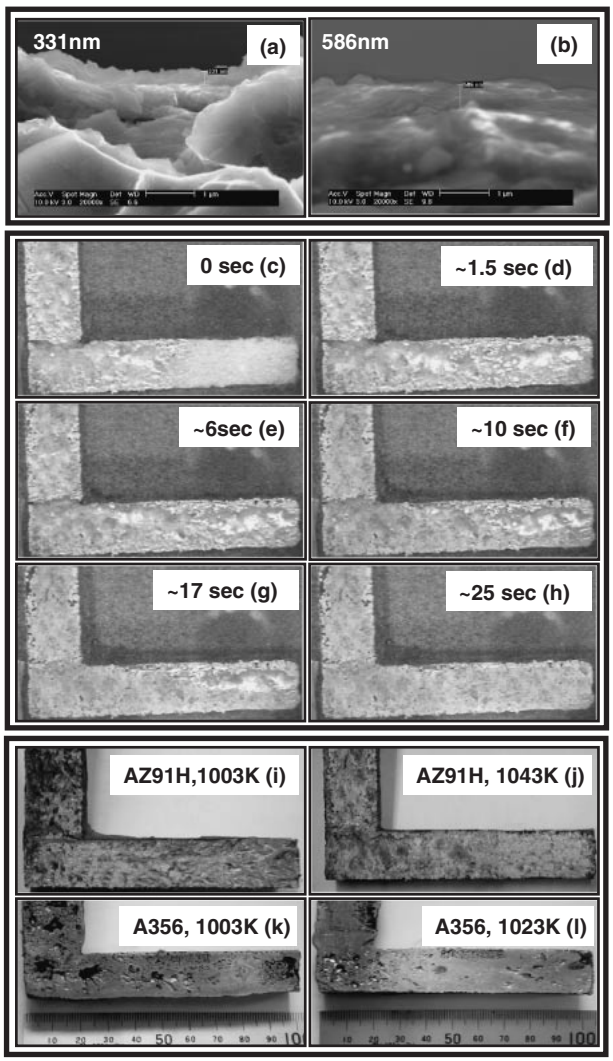

Fig. 9 (a–b) SEM images showing the oxide film thickness for A356 and AZ91H alloy in LFC, (c–h) photographs showing the filling behavior of AZ91H Mg alloy in test casting-L, (i–l) photographs showing the surface morphologies after test casting-L for A356 and AZ91H alloys.

thus, the melt has many possibilities of entrapping the pyrolysis products. Consequently, this argument cannot explain the difference in the porosity concentration of both alloys. The second argument focuses on the surface energy difference between the liquid metal and the entrapped gas for both alloys. With a pore size of about 10 μm, the AZ91H alloy has a much smaller pore size than the A356 alloy, which is about 1 mm. Based on the following equation, the free surface energy for the AZ91H alloy must be larger than that of the A356 alloy:

$$P_i \geq P_{atm} + P_H + \gamma(1/r_1 + 1/r_2) \quad (4)$$

where P_i is the internal pressure for a pore, P_{atm} is the atmospheric pressure on the melt surface, P_H is the metallostatic head pressure, and $\gamma(1/r_1 + 1/r_2)$ is the force due to the surface tension. However, the real free surface energy for the AZ91H alloy at 973 K, γ_{sv}, is 550 mJ/m^2, which is smaller than the 1080 mJ/m^2 for the A356 alloy.[12–14] The third argument examines the characteristic differences in the solubility of both alloys. This approach is reasonable

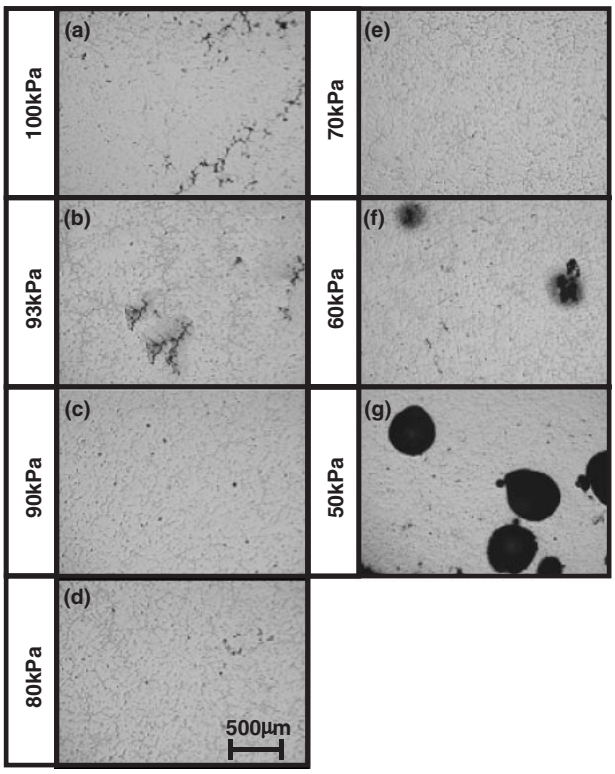

Fig. 10 Macrostructures of 11 mm-thick samples with different casting pressures.

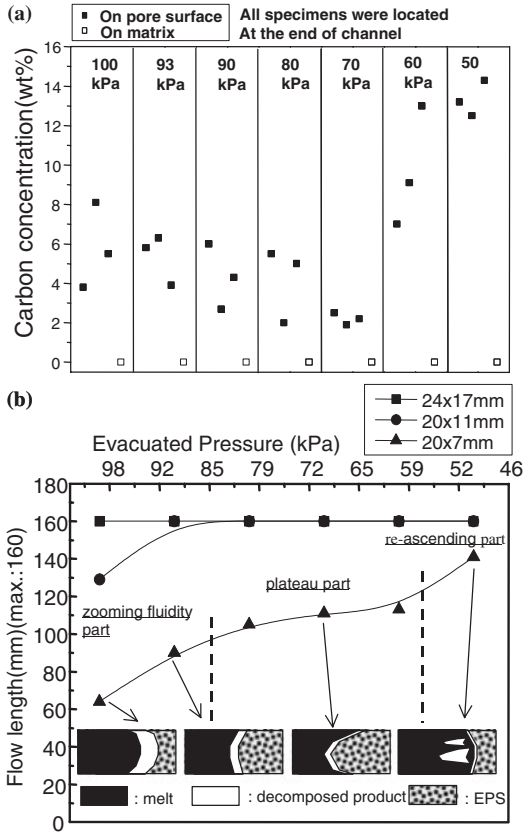

Fig. 11 (a) Carbon concentrations on pore surfaces of castings with different mold evacuation pressures, (b) the fluidities of AZ91H alloy in test casting-T under various casting pressures and the model of filling mechanism according to evacuation pressures.

because the AZ91H alloy has enough extra hydrogen concentration for the solubility limit at the solidus temperature, and the hydrogen gas that originates from the entrapped products can be dissolved into the melt. However, because the level of the hydrogen solubility limit for the A356 alloy is near zero, the hydrogen that originates from a source such as the entrapped polymer can easily approach the solubility limit in the melt. This argument is supported by Figs. 9(c)–(h), which shows the visible melt filling and solidification processes that we viewed with the aid of the digital camera in the Test Casting-L.

After complete filling [Fig. 9(h)], the formed gas clusters coarsened and contracted over time. Figs. 9(i)–(l) shows the surface morphologies after the casting of both alloys for the Test Casting-L. See Figs. 9(i)–(j) for the AZ91H alloy and Figs. 9(k)–(l) for the A356 alloy. It is obvious that the AZ91H alloy forms fewer pores than the A356 alloy.

Figure 10 shows how mold evacuation affects pore formation. As the vacuum degree increases from 100 to 90 kPa, the amount of pores and shrinkage defects decrease. We observed almost no pores at 70 kPa. The mold evacuation seems to improve the fluidity of the melt. However, the high amount of pores occurs at a severe low pressure, such as 60 and 50 kPa, as shown in Figs. 10(f)–(g), and the severe low pressure is caused by the large entrapment of the pyrolysis products, the mechanism of which is demonstrated in Fig. 11(b).

Figure 11(a) shows our analysis of the carbon concentration on the pore surface at various vacuum degrees. The carbon concentration decreases as the evacuation pressure decreases to 70 kPa. This decrease means that the pyrolysis products are easily able to escape under evacuation. In turn, the carbon concentration increases from 60 to 47 kPa because of the severe entrapment for the pyrolysis products. Figure 11(b) shows the fluidity of the AZ91H alloy and the metal filling mechanism under different vacuum degrees in the LFC. The fluidity characteristic that depends on the vacuum degree has three parts: the zooming fluidity, the plateau and the re-ascending parts. The fluidity increased dramatically with the increasing vacuum degree in the zooming part (100 to 80 kPa). In addition, because the smaller pressure gradient forward of the pattern wall pulls the metal front over a very limited length, the polystyrene pyrolysis products at the metal-pattern interface can be more easily pushed to the metal-polystyrene pattern-coating interface and extracted to the outside of the mold cavity. With a further increase in the degree of the vacuum, the metal front at the pattern wall will extend even longer so that the pyrolysis products of the center pattern must take a longer route to get to the metal-pattern-coating interface. As a result, the products are removed to the outside of the mold cavity; hence, the increase of fluidity slows down between 80 and 60 kPa in the plateau. When the vacuum degree is higher than a critical value, 60 kPa, the metal front on the pattern wall is longer than the metal front at the pattern center.

On the other hand, the central pattern of the pyrolysis products becomes a stumbling block to the melt flow because the liquid products that adhere to the front of the melt inhibit

the flow of the melt. Furthermore, the liquid products gasify and form back pressure at the melt front. As a result, the melts that flow from both walls meet each other in the center of the pattern ahead of the metal front; again, the fluidity increases abruptly (at the re-ascending part). Nonetheless, the liquid products trapped in the melt leave behind a high amount of pores in the cast, as shown in Figs. 10(f)–(g). This argument supports the proposition of Liu *et al.*[2] However, if we graphically redraw the argument of Liu *et al.* together with our results for carbon concentration, the model will resemble Fig. 11(b).

4. Conclusions

The pore formation characteristics that occur in the LFC of the AZ91H alloy were investigated with reduced pressure and atmosphere castings, and we compared our results with the results of the previous work for the A356 alloy.

(1) Under normal humidity, the AZ91H alloy melt has an extra hydrogen concentration for the hydrogen solubility limit at the solidus temperature. This extra hydrogen concentration produces a total porosity ranging from 0.05 to 0.38 vol%, which is lower than the total porosity of the A356 alloy, which ranges from 0.6 to 2.2 vol%. The poor fluidity of the AZ91H alloy melt increases with the pouring temperature (1073 K) to induce the minimum porosity, which is as high as 323 K for the A356 alloy.

(2) The pore formation mechanism for the AZ91H alloy is similar to that of the A356 alloy. However, the transition temperature, which reveals a different mechanism, is higher in the AZ91H alloy than in the A356 alloy due to the worse fluidity of the AZ91H alloy.

(3) A proper evacuation pressure produces the minimum porosity, and the vacuum degree that exceeds the critical pressure leaves behind many pores because of the severe entrapment of the polystyrene pyrolysis products.

Acknowledgements

The authors wish to thank the financial support of KMAC and BK21 Project of Korean Government.

REFERENCES

1) H. F. Shroyer: U. S. Patent No. 2,830,343, April 15 (1958).
2) Z. Liu, J. Hu, Q. Wang, W. Ding, Y. Zhu, Y. Lu and W. Chen: J. Mater. Process. Tech. **120** (2002) 94–100.
3) I. M. Park, J. C. Choe and T. W. Nam: Korea Foundrymens Society **12** (1992) 285–290.
4) R. P. Walling and J. A. Dantzig: AFS Trans. **102** (1994) 849–854.
5) L. Wang, S. Shivkumar and D. Apelian: AFS Trans. **98** (1990) 923–933.
6) S. R. Shin, S. W. Han, K. W. Lee and Z. H. Lee: J. Korean Foundrymens Society **23** (2003) 268–275.
7) S. R. Shin, H. J. Choi, K. H. Lee and Z. H. Lee: J. Mater. Sci. **39** (2004) 1563–1569.
8) S. R. Shin, H. J. Choi, K. H. Lee and Z. H. Lee: J. Korean Foundrymens Society **22** (2002) 167–173.
9) E. F. Emley: *Principles of Magnesium Technology*, (Pergamon Press, First edition, 1966) p. 193.
10) F. Sauerwald: Z. Anorg. Chem. **258** (1945) 27.
11) P. N. Anyalebechi: Scr. Metall. Mater. **33** (1995) 1209–1216.
12) H. Jones: *The surface energy of solid metals*, (1971) p. 15.
13) E. F. Emley: *Principle of Magnesium Technology*, (Pergamon Press, First edition, 1966) p. 24.
14) L. Kubichek and M. V. Maltesy: Met. Abs. **28** (1960) 28.